Engenharia Agrícola

ISSN: 1809-4430 (on-line)

www.engenhariaagricola.org.br

Scientific Paper
Doi: http://dx.doi.org/10.1590/1809-4430-Eng.Agric.v43n3e20220062/2023

A ROTARY BLADE DESIGN FOR PADDY FIELDS WITH LONG RICE STRAW BASED ON EDEM

Chengcheng Ma[1], Shujuan Yi[1*], Guixiang Tao[1]

[1*]Corresponding author. College of Engineering, Heilongjiang Bayi Agricultural University, Daqing, China.
E-mail: yishujuan_2005@126.com | ORCID ID: https://orcid.org/0000-0003-1708-0839

KEYWORDS

agricultural engineering, rotary blade of paddy field, EDEM, parameter optimization, performance test.

ABSTRACT

The paddy field machine uses excessive power during paddy field preparation because of the high distribution density of rice straw. In this study, a rotary blade is created to address this problem. The structural parameters of the rotary blade were designed and the dynamic analysis of the rotary blade's soil-cutting process was completed to establish a model of the rotary blade's power consumption. Through the model, the primary factors influencing the rotary blade's power consumption were identified. A composite soil bin model of rice straw–muddy layer–bottom soil was established in EDEM software, with the bending angle of the front blade, the working width of a single blade, and the thickness of the blade as the test factors. The straw burying rate, power consumption, and surface flatness after rotary tillage were used as evaluation indicators to conduct multi-factor simulation tests on the composite soil bin model. The optimized analysis of the test data showed that the optimal geometric parameters for the rotary blade were 49 mm working width, 108° front blade bending angle, and 4 mm blade thickness. A field verification test was carried out on the optimized rotary blade, and the test results showed that the surface flatness after rotary tillage was 3.25 cm, the qualified rate of rotary tillage depth was 93.3%, and the degree of mud mixing was 3.41 kg/dm^3, which was suitable for the land preparation requirements of paddy fields.

INTRODUCTION

China's rice planting area has grown to 30.15 million hectares with an annual output of 204 million tons, placing it second in the world. However, there are still some obstacles to the mechanization of paddy fields that need to be addressed immediately, especially in the preparation of paddy fields with long rice straw. After the rice harvest, the long rice straw that remains cannot be adequately treated (Zhu et al., 2016).

Currently, most paddy fields fill the straw with rotary tillage, which is inefficient and the machine's power consumption is greater (Konno et al., 2016). Some researchers have conducted a series of studies on the technology and methods of using paddy field machines in light of the current scenario of paddy field preparation with long rice straw (Xin et al., 2019; Efremov & Nasonov, 2016; Bai, 2010).

Matin et al. (2016) conducted some simulation analysis based on the radius of the rotary blade surface, the forward speed of the machine, and the rotational speed of the blade roll, based on the construction of a flattening and puddling paddy field machine. They investigated a leveling device designed by Hu et al. (2020) and Zhou et al. (2020). Shrivastava &Verma (2017) used the Taguchi method to optimize jigs and fixtures for rice weeder production, which saved 60% of the weeding cost and 65% of the time compared to human weeding. In terms of tillage, Mousavi et al. (2009) explored the influence of the puddling intensity on the physical qualities of silty clay in the lab and in the field and discovered that moderate intensity is best for tillage in silty clay paddy fields.

However, there have been few investigations into rotary blade performance in paddy fields with long rice straw. As a result of this study, a rotary blade was developed that is ideal for paddy fields with long rice straw. The

[1] College of Engineering, Heilongjiang Bayi Agricultural University, Daqing, China.

Area Editor: Teresa Cristina Tarlé Pissarra
Received in: 4-18-2022
Accepted in: 6-26-2023

operating principle is explained, as is the creation of a mathematical model and the design of the required parameters. This paper provides a guide for developing critical components for paddy fields with long rice straw.

MATERIAL AND METHODS

Structure and operation of a paddy field machine

The paddy field machine is mainly composed of the rotary blade, shaft of the rotary blade, gearbox, and cover plate. The schematic diagram of the device is shown in Figure 1.

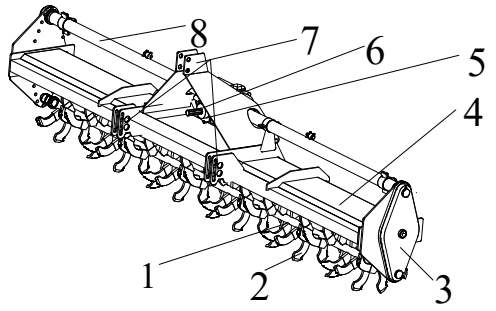

1. Rotary blade roller; 2. rotary blade; 3. gearbox on the side; 4. cover plate; 5. gearbox; 6. input shaft for power; 7. three-point hitch; 8. lateral drive shaft

FIGURE 1. Schematic diagram of the paddy field machine.

The mechanism operates as follows: the tractor's power output shaft drives the rotary blade roller to rotate at a high speed. The rotary blade can bury the stubble by pushing the long straw remaining on the mud surface into the mud.

Power consumption analysis of paddy field machine

The transmission portion of the paddy field machine, overcoming the horizontal reaction force acting on the soil, cutting the soil, and throwing the soil, makes up the majority of the power consumption of the rotary blade. The paddy field machine uses the following amount of power overall:

$$N = N_q + N_p + N_n + N_f \tag{1}$$

in which:

N_q is the power consumed by cutting the soil (kW);

N_p is the power consumed by throwing the soil (kW);

N_n is the power consumed by overcoming the horizontal reaction force of the soil (kW), and

N_f is the power consumed by the transmission (kW).

The paddy field machine's rotating blades plow the soil by rotating around the blade shaft and moving forward. The throwing and cutting of the soil take place simultaneously. The power of the paddy field machine used for cutting the soil can be expressed as:

$$N_q = \frac{1}{75} A_q B v_m \tag{2}$$

in which:

A_q is the specific work of cutting the soil (N/cm^2);

B is the working width (mm), and

v_m is the forward speed (m/s).

Under the influence of the rotary blade, the movement of the soil is extremely complicated. The soil condition, the size, shape, and condition of the soil block, as well as the rotary blade's shape and size, all affect the direction and rate of soil movement. The rotary blade's power to throw the soil is denoted by:

$$N_p = \frac{1}{75} A_p a B v_m \omega^2 R^2 \tag{3}$$

in which:

A_p is the specific work of throwing the soil (N/cm^2);

ω is the rotational angular velocity of the rotary blade (rad·s^{-1});

a is the rotary tillage depth (mm), and

R is the rotary blade's rotational radius (mm).

The force acting on the rotary blade is shown in Figure 2, and the power consumed by overtaking the horizontal reaction force of the soil (N_n) is the power consumed to overcome the reaction force of the soil acting on the rotary blade in the horizontal direction.

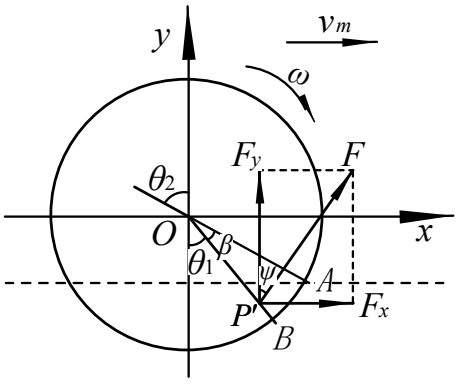

FIGURE 2. Force analysis of rotary blade.

The resistance torque of the blade shaft, m, is created by the resistance torque of each individual rotary blade that is successively inserted into the soil. Assume that the average resistance F of the soil acting on the rotary blade is evenly distributed on the rotary blade. The radius of action of the resultant resistance force when the rotary blade's end point cuts the soil with a radius of gyration R is R'=0.9R, and F=m/R'. The center of the blade shaft O is the center of the circle, and the rotary blade's maximum radius of gyration is the radius to make a circle. At point A, where the circle's horizontal axis and the surface of the cultivated land intersect, the rotary blade's entry angle is ψ at this time. With respect to the radius line OA, we make the radius line OB whose intersecting angle is the cutting angle β (β<0), determine the point P' at 0.9R on the OB, and set the force F acting point at the point P'. As a result of the analysis in Figure 2, we learn that:

$$\begin{cases} \theta_2 = 90° - \psi = \theta_1 + \beta \\ F_y = F \sin\theta_2 \\ F_x = F\cos\theta_1 = F\cos(90° - \psi - \beta) \end{cases} \tag{4}$$

in which:

F is the average resistance of the soil on the rotary blade, (N);

ψ is the entry angle of the rotary blade, (°), and

β is the angle of cutting, (°).

Then the formula of the rotary blade to overcome the soil horizontal reaction force consumption power, N_n, can be expressed as:

$$N_n = F_x v_m \tag{5}$$

The paddy field machine's transmission part's loss power, N_f, can be expressed as follows:

$$N_f = (1-\eta)(N_q + N_p + N_n) \tag{6}$$

in which:

η is the transmission efficiency.

In conclusion, the rotary blade's power consumption can be expressed as follows:

$$N = (2-\eta)(\frac{1}{75} A_q a B v_m + \frac{1}{75} A_p H B v_m \omega^2 R^2 + F_x v_m) \tag{7}$$

From Formula (7), it is clear that the machine's forward speed, the rotary blade's rotational speed, the rotary tillage depth, and the rotary blade's working width and rotational radius will all have an impact on the power consumption.

Curved side blades

Gupta & Singh (2012) evaluated the five curves of the Archimedes spiral, equiangular spiral, and sinusoidal exponential curve and discovered that the Archimedes spiral had the lowest tillage resistance, hence it was chosen as the curve of the rotary blade's side blade. Figure 3 shows a schematic representation that can be stated as Formula (8).

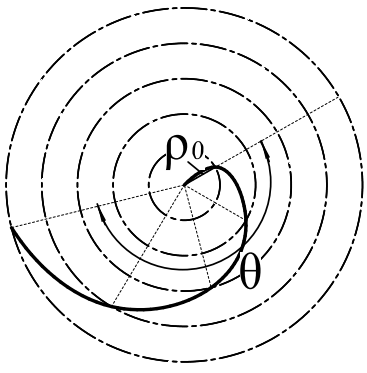

FIGURE 3. Archimedes spiral schematic.

$$\rho = \rho_0 + a' \cdot \theta \tag{8}$$

in which:

ρ_0 is the diameter of the spiral's beginning point's pole (mm);

a' is an increase in pole diameter associated with each increase in the screw pole angle (mm), and

θ is the spiral's pole angle at any position (rad).

(1) Calculation of ρ_0

The pole diameter (ρ_0) of the spiral's beginning point can be represented as Formula (9) to avoid cutting the soil without blades.

$$\rho_0 = \sqrt{R^2 + S^2 - 2S\sqrt{2Ra - a^2}} \tag{9}$$

in which:

S is the pitch of the soil-cutting rotary blade (mm).

The rotational radius, the pitch of the rotary blade cutting the soil, and the depth of rotary tillage by the rotary blade are all connected to the pole diameter.

① Rotary blade's rotational radius (R)

The structure of the rotary blade in this study is a scimitar type, which is suited for paddy field green manure, rice straw, and wheat straw. Scimitars have five rotational radius (R) standards: 195 mm, 210 mm, 225 mm, 245 mm, and 260 mm. The rice straw must be buried 100 mm below the soil surface to meet agronomic criteria. The rotational radius of the corresponding rotary blade ranges from 240 mm to 260 mm, and was therefore chosen as 245 mm based on traditional design experience.

② Rotary tillage depth (a)

The depth of rotary tillage was required to be between 100 mm and 200 mm according to the *Technical Regulations for Paddy Field Rotary Tillage (DB21/T1672-2019)*, so 150 mm was chosen for the depth in this study (a=150 mm).

③ Pitch of the soil-cutting rotary blade (S)

The number of rotary blades on the shaft in the same plane was set to two to improve the performance of stirring the mud. The pitch of the soil-cutting rotary blade can be set as shown in Formula (10).

$$S = v_m t = \frac{2\pi \cdot v_m}{z\omega} = \frac{2\pi \cdot R}{z\lambda} \tag{10}$$

in which:

z is the number of rotary blades on the tool axis that are installed in the same plane;

λ is the rotary tillage speed rate (rad), and

t is the time interval between successive breakage of two adjacent rotary blade(s).

The speed rate of rotary tillage (λ) was defined as the ratio of the rotary front speed at the end point of the rotary blade to the forward speed of the rotary blade, as indicated in Formula (11).

$$\lambda = R\omega / v_m \tag{11}$$

in which:

λ is the speed rate of rotary tillage (rad);

R is the rotational radius for the rotary blade (mm);

ω is the rotating angular velocity of the rotary blade (rad·s^{-1}), and

v_m is the forward speed of the rotary blade (km/h).

The locomotive operating speed (v_m) is required to be 2~5 km/h, the tractor power output shaft speed (ω) is 540~720 r/min, and the speed rate of rotary tillage (λ) of Formula (11) is 1.65.3 rad (λ=1.65.3 rad), according to the *Technical Regulations for Paddy Field Rotary Tillage (DB21/T1672-2019)*. Formula (11) is incorporated into Formula (10) to achieve the 150~480 mm (S=150~480 mm) pitch of the rotary blade cutting the soil. The smaller the cutting pitch, the better the performance of stirring the mud, so the pitch of the rotary blade cutting the soil is selected as 150 mm (S=150 mm) based on the soil characteristics. We put S=150 mm, R=245 mm, and a=150 mm into Formula (9) to get the pole diameter of 122 mm (ρ_0=122 mm).

(2) Calculation of a'

An increase in the pole diameter (a') is seen in Formula (12) when the spiral pole angle increases by 1 radian.

$$a' = (\rho_n - \rho_0)/\theta \tag{12}$$

in which:

ρ_n is the pole diameter at the end point for the spiral (mm);

θ is the pole angle at the end point for the spiral (°), and

ρ_0 is the pole diameter at the starting point for the spiral (mm).

As a result, the increment in the pole diameter (a') is determined to be related to the pole diameter at the end point for the spiral (ρ_n), the pole angle at the end point for the spiral (θ), and the pole diameter at the spiral's starting point (ρ_0).

① Pole diameter at the end for spiral (ρ_n)

The value of ρ_n was 10~20 mm less than the rotational radius of the rotary blade in order to make the spiral transition smoothly with the front edge, thus here ρ_n =245-20=225 mm.

② Pole angle at the end point for spiral (θ)

The polar angle at the spiral's termination point is represented by Formula (13).

$$\theta = \frac{\rho_n - \rho_0}{\rho_n} \tan \tau_n \tag{13}$$

in which:

τ_n is the sliding cut angle of the end for the spiral (static), (°).

The end of the rotary blade's static sliding cut angle is normally 50° to 60°. A rotary blade with a larger static sliding cut angle has a longer blade length and, while cutting soil, the friction surface with the soil increases, increasing the tillage resistance; therefore, the value selected for n was 50° (n=50°). Using Formula (13) and the values ρ_n = 225 mm, ρ_0 = 122 mm, and τ_n = 50°, the pole angle at the end of the spiral is 31.5° (θ=31.5°), and a'=3.27 is found using Formula (12). In Formula (8) the values of a', ρ_n, and ρ_0 were replaced, and the formula for the side blade curve was ρ=122+3.27θ, as illustrated in Figure 4.

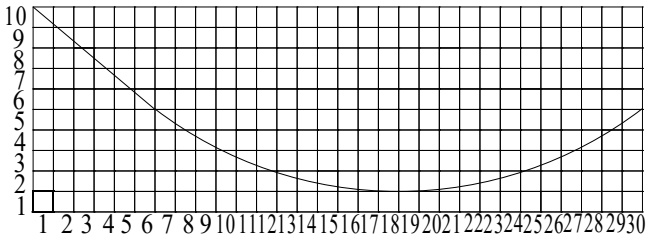

FIGURE 4. Side blade curve of the rotary blade.

Curve of the front blade

The design uses the front edge as the spatial curve, according to the *Agricultural Machinery Design Manual* and existing literature (Zhou et al., 2020; Shrivastava and Verma, 2017; Anisa and Geeta, 2017; Matin et al., 2016). The front blade and the side blade were seamlessly transitioned by a circular arc line, as shown in Figure 5a.

Curve of the transitional blade

The national standard for transitional blades uses a radius of 30 mm (R_c=30 mm) to connect the curve of the side blade and the curve of the front blade, as shown in Figure 5b, where γ is the bending angle of the front blade, W_b is the single blade's working width, and b is the thickness of the blade.

The working sketch of the rotary blade is shown in Figure 5c.

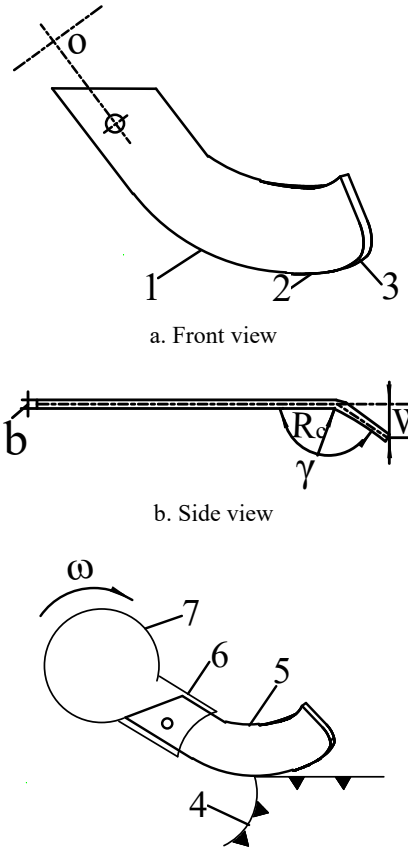

a. Front view

b. Side view

c. Working sketch of rotary blade

1. Curve of side blade (ρ=122+3.27θ); 2. curve of transitional blade; 3. curve of front blade; 4. soil; 5. rotary blade; 6. blade holder; 7. blade shaft

Note: working width of single blade (W_b=20~60 mm); bending angle of front blade (γ=100~140°); thickness of blade (b=3.5~5.5 mm).

FIGURE 5. Structure and working sketch of rotary blade.

SIMULATION EXPERIMENT

In this study, the discrete element method is used to simulate paddy field straw returning to the field (Azimi-Nejadian et al., 2022; Ucgul and Saunders, 2020; Zhao et al., 2020). Multi-factor experiments were carried out on the rotary blade's different geometric sizes by simulation in order to investigate the influence of these sizes on the rate of burying straw, the flatness after rotary tillage, and power consumption, and then the best geometric parameters of the rotary blade were obtained.

A soil bin model

Shi et al. (2019) chose a paddy field with long rice straws as the subject of study. As indicated in Table 1, Hwang (2011) used electronic scales and other devices to measure the parameters of the mud, rice straw, and bottom soil. The mud and bottom soil depths are respectively 0~50 mm and 50~200 mm. The soil bin's overall length, breadth, and height are 2000 mm, 500 mm, and 250 mm, respectively, as illustrated in Figure 6. Figure 7 depicts the simulation process diagram.

TABLE 1. Parameters for simulation materials.

Type of material	Density/(kg·m^3)	Poisson ratio	Shear modulus/(Pa)
Rice straw	241	0.40	1×10^6
Muddy layer	1500	0.38	1×10^6
Bottom soil	1850	0.30	1×10^8

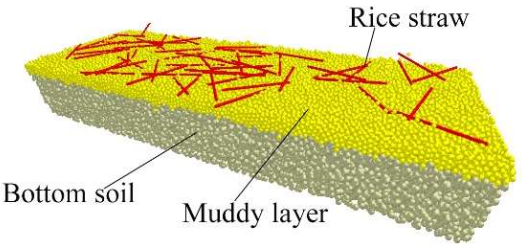

FIGURE 6. Soil bin model.

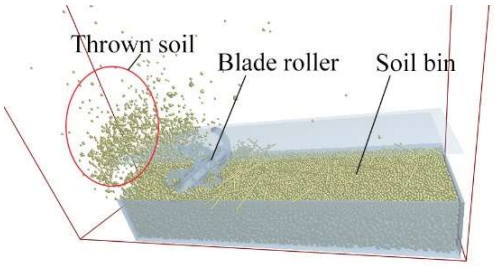

FIGURE 7. Simulation procedure.

Determination of simulation model parameters

The Hertz–Mindlin contact model with JKR was used to simulate the interaction between the mud and bottom soil due to the viscosity of the mud and soil. Virtual simulation calibration and reference literature were used to determine the dynamic and static friction coefficients and restitution coefficients of No. 45 steel–mud, mud–mud, and rice stalk–rice stalk contact models. Table 2 shows the values of the associated parameters.

TABLE 2. Simulation contact parameters.

Type of interactive material	Collision recovery factor	Coefficient of static friction	Dynamic friction coefficient
Rice straw–rice straw	0.3	0.9	0.1
Muddy layer–muddy layer	0.3	0.114	0.1
Bottom soil–bottom soil	0.6	0.6	0.4
Muddy layer–rotary blade	0.5	0.2	0.03
Rice straw–rotary blade	0.2	0.3	0.01
Rice straw–muddy layer	0.4	0.8	0.2
Muddy layer–rotary blade	0.6	0.6	0.05
Muddy layer–rice straw	0.4	0.8	0.2

Test factors, indicators and test methods

The working width of a single blade, the bending angle of the front blade, and the blade thickness were the test factors. The rice straw burial rate, surface flatness after rotary tillage, and power consumption were chosen as test indicators.

The power consumption with different geometric parameters can be achieved by processing power consumption performance index data and outputting the torque of the blade roller through the ‘create graph’ function in the post-processing module, as shown in Figure 8a. The ruler function is used to survey and map the simulated flatness data after the plowing the ground surface flatness performance index data, as shown in Figure 8b. The top view of the stubble is observed to acquire the amount of rice straw floating in the upper layer from the stubble burying rate performance index data, and then the stubble burying rate after rotary tillage is computed, as illustrated in Figure 8c.

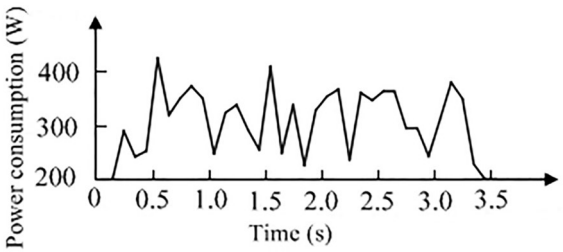

a. Power consumption of blade roller

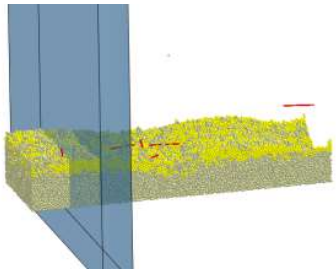

b. Schematic diagram of measuring flatness

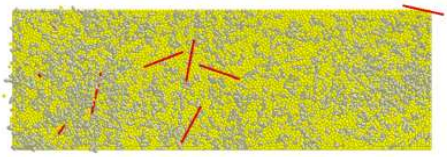

c. Schematic diagram of post-processing after measuring stubble burying rate

FIGURE 8. Schematic diagram of measurement test performance data.

RESULTS AND DISCUSSION

Results

Table 3 shows the level code of each factor from an experiment with a three-factor and five-level quadratic rotation orthogonal combination design. By consulting *Rotary tiller - Rotary blades and blade holders* and taking into account the actual blade size, the levels of each test factor are established.

TABLE 3. Level code of each factor from a three-factor and five-level design.

Code	Working width of single blade (mm)	Bending angle of front blade (°)	Thickness of blade (mm)
1.682	60.00	140.00	5.50
1	51.89	131.89	5.10
0	40.00	120.00	4.50
-1	28.11	108.11	3.91
-1.682	20.00	100.00	3.50

Table 4 shows the 23 test schemes and results of the quadratic regression orthogonal rotation combination design, where x_1 is the single blade's working width, x_2 is the front blade's bending angle, x_3 is the blade thickness, y_1 is the rice straw burying rate, y_2 is the surface flatness after rotary tillage, and y_3 is the power consumption.

TABLE 4. Design scheme and results of quadratic orthogonal rotation combination.

Number	Experimental factors			Performance indexes		
	x_1	x_2	x_3	y_1	y_2	y_3
1	-1	-1	-1	0.783	57.9	269.43
2	1	-1	-1	0.850	45.5	297.97
3	-1	1	-1	0.783	78.4.	362.43
4	1	1	-1	0.783	65.5	406.79
5	-1	-1	1	0.783	69.5	418.51
6	1	-1	1	0.900	53.0	436.94
7	-1	1	1	0.817	69.8	395.33
8	1	1	1	0.850	61.0	481.97
9	-1.682	0	0	0.783	63.2	388.40
10	1.682	0	0	0.85	42.8	445.09
11	0	-1.682	0	0.85	50.5	330.03
12	0	1.682	0	0.783	72.3	434.87
13	0	0	-1.682	0.783	44.2	272.25
14	0	0	1.682	0.850	71.7	445.03
15	0	0	0	0.800	35.3	406.83
16	0	0	0	0.867	36.2	399.12
17	0	0	0	0.900	41.8	381.19
18	0	0	0	0.867	32.2	403.64
19	0	0	0	0.867	37.3	394.05
20	0	0	0	0.867	35.1	408.63
21	0	0	0	0.883	41.8	396.36
22	0	0	0	0.867	32.8	416.46
23	0	0	0	0.867	30.8	396.48

Discussion

Table 5 reveals that the interaction between a single blade's operating width and the front blade's bending angle had a substantial impact on the rice straw burying rate and power consumption. The response surfaces of the interaction between the working width of a single blade and the bending angle of the front edge on the burying rate of rice straw and power consumption, as illustrated in Figures 9 and 10, were obtained using software for Design-Expert 8.0.6.

TABLE 5. Analysis of variance on outcome data.

Source of variance	Quadratic sum (SS)	Degrees of freedom (DF)	Mean square (MS)	Variance rate	Significance probability
Pattern	0.032	9	0.0036	7.25	0.0008
x_1	0.0080	1	0.0080	16.18	0.0014
x_2	0.0028	1	0.0028	5.7	0.0328
x_3	0.0051	1	0.0051	10.35	0.0067
x_1x_2	0.0029	1	0.0029	5.8	0.0317
x_1x_3	0.0009	1	0.0009	1.75	0.2086
x_2x_3	0.0003	1	0.0003	0.66	0.4308
x_1^2	0.0041	1	0.0041	8.37	0.0126
x_2^2	0.0041	1	0.0041	8.37	0.0126
x_3^2	0.0041	1	0.0041	8.37	0.0126
Residual error	0.0064	13	0.0005		
Misfit item	0.0006	5	0.0001	0.16	0.9688
Pure error	0.0058	8	0.0007		
Total value	0.038	22			
Pattern	4790.07	9	532.23	19.20	<0.0001
x_1	527.90	1	527.90	19.04	0.0008
x_2	534.82	1	534.82	19.29	0.0007
x_3	199.90	1	199.90	7.21	0.0187
x_1x_2	6.48	1	6.48	0.23	0.6368
x_1x_3	0.00	1	0.00	0.00	1.0000
x_2x_3	129.61	1	129.61	4.67	0.0498
x_1^2	741.18	1	741.18	26.73	0.0002
x_2^2	1525.91	1	1525.91	55.04	<0.0001
x_3^2	1169.69	1	1169.69	42.19	<0.0001
Residual error	360.43	13	27.73		
Misfit item	238.45	5	47.69	3.13	0.0739
Pure error	121.98	8	15.25		
Total value	5150.50	22			
Pattern	61543.31	9	6838.15	67.79	<0.0001
x_1	5469.69	1	5469.69	54.22	<0.0001
x_2	11715.09	1	11715.09	116.14	<0.0001
x_3	34529.98	1	34529.98	342.32	<0.0001
x_1x_2	882.63	1	882.63	8.75	0.0111
x_1x_3	129.36	1	129.36	1.28	0.2779
x_2x_3	4048.65	1	4048.65	40.14	<0.0001
x_1^2	484.33	1	484.33	4.80	0.0473
x_2^2	693.00	1	693.00	6.87	0.0211
x_3^2	3585.71	1	3585.71	35.55	<0.0001
Residual error	1311.33	13	100.87		
Misfit item	491.24	5	98.25	0.96	0.4950
Pure error	820.09	8	102.51		
Total value	62854.64	22			

Figure 9 shows that, as the working width of a single blade and the bending angle of the front blade are increased, the stubble burying rate initially increases and then declines. When the operating width of a single blade is fixed, the burying rate of rice straw first increases and then drops when the bending angle of the front blade increases. When the bending angle of the front blade is fixed, the burying rate of rice straw increases as the operating width of the blade grows.

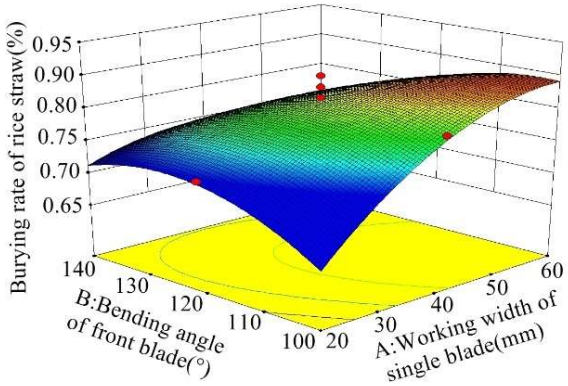

FIGURE 9. Impact of interplay between working width of single blade and bending angle of front blade on the burying rate of rice straw.

Figure 10 shows that as the working width of a single blade and the bending angle of the front blade are increased, the power consumption also increases. When the operating width of a single blade is fixed, the power consumption increases as the bending angle of the front blade increases. When the bending angle of the front blade is fixed but the operating width of a single blade increases, the power consumption tends to increase.

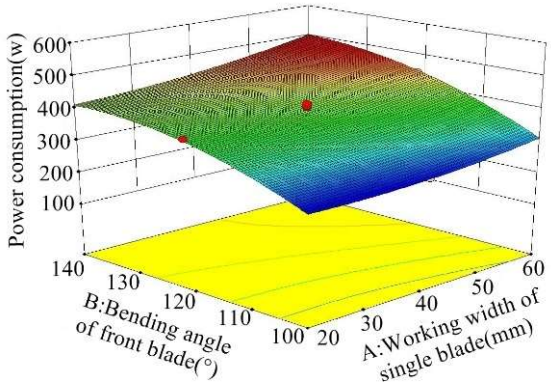

FIGURE 10. Impact of interplay between working width of single blade and bending angle of front blade on power consumption.

The rice straw burial rate, surface flatness after rotary tillage, and power consumption were optimized using the Design-Expert 8.0.6 software, and the nonlinear formula is shown in Formula (14).

$$\begin{cases} \max Y_1 \\ \min Y_2 \\ \min Y_3 \\ \text{s.t. } 20\text{mm} \le x_1 \le 60\text{mm} \\ 100° \le x_2 \le 140° \\ 3.5\text{mm} \le x_3 \le 5.5\text{mm} \end{cases} \quad (14)$$

The ideal size parameter combination for the rotary blade was also optimized and determined using Design-Expert 8.0.6 software, giving the operating width of a single rotary blade of 48.6 mm, the front blade's bending angle of 108.1°, and the blade thickness of 4.1 mm.

The optimized rotary blade was installed on the paddy field machine to perform a field test to evaluate the outcome. Prior to the test, the experimental field's rice straw had a density of 167.49 g/m^2, a length of 151 mm, and a moisture content of 7.10%. The paddy field machine was mounted on a Dongfanghong 904 tractor. The machine's working width was 3.6 m, its fixed working depth was 12 cm, its forward speed was 1.6 km/h, and the rotary blade roller's rotational speed was 300 rpm. The data for surface flatness after rotary tillage was measured and calculated using a 3 m ruler and standard deviation formula, while the data for the qualified rate of the rotary tillage depth, the degree of mud mixing, and the rate of burying rice straw were measured using the five-point sampling method. The measured performance index data was compared to the quality standards of the *Technical Specification for Paddy Field Rotary Tillage (DB21/T 1672-2019)* in order to test the performance of the proposed rotary blade following rotary tillage. Figure 11 depicts the field experiment measurement technique. Table 6 displays the comparison data.

FIGURE 11. Field experiments measurement technique.

TABLE 6. Comparison of the performance indicators before and after.

Testing indicators	Technical procedure and operating requirements	Indicator values
Burying rate of rice straw (%)	≥80	92.2
Surface flatness after rotary tillage (cm)	≤5	3.25
Qualified rate of rotary tillage depth (%)	≥90	93.3
Degree of mixing mud (kg/m^3)	≤5	3.41

As shown in Table 6, the planned paddy field rotary blade buried the rice straw at a rate of 92.2%, an increase of 12.2% over the operating quality standards of the technical procedures. After rotary tillage, the surface flatness was reduced by 1.75 cm. In comparison to the technical processes, the qualified rate of rotary tillage depth increased by 2.0%. The amount of mixed mud was reduced by 1.59 kg/m^3.

CONCLUSIONS

(1) A rotary blade suitable for paddy field preparation was designed. The blade curve, dynamic sliding angle, and other parameters of the rotary blade were theoretically analyzed and designed. By establishing the power consumption model, the experimental factors of the rotary blade such as the working width of a single blade, the bending angle of the front blade, and the blade thickness were obtained.

(2) A composite soil bin model made up of rice straw–muddy layer–bottom soil was established using the discrete element method. The rotary blade designed was simulated in the soil bin model. Using the quadratic regression orthogonal rotation combined test and response surface combined test methods, the working width of a single blade, the bending angle of the front blade, and the blade thickness as the test factors, the rice straw burying rate, surface flatness after rotary tillage, and power consumption form a quadratic regression mathematical model for evaluation indicators. The regression equations for the rice straw burying rate, surface flatness after rotary tillage, and power consumption were optimized and solved using Design-Expert 8.0.6 software. The results show that the optimal parameters are 49 mm working width of a single blade, 108° bending angle of the front blade, and 4 mm blade thickness.

(3) Field tests were carried out to verify the optimal structural parameters of the rotary blade. The surface flatness after rotary tillage was 3.25 cm, the qualified rate of rotary tillage depth was 93.3%, and the degree of mixing mud was 3.41 kg/dm^3, which satisfied the paddy field preparation standards.

REFERENCES

Anisa A, Geeta G (2017) Performance testing of the rotary paddy weeder with different angle of blade. International Journal of Agricultural Engineering 10(1): 86-91. https://doi.org/10.15740/HAS/IJAE/10.1/86-91

Azimi-Nejadian H, Karparvarfard SH, Naderi-Boldaji M (2022) Weed seed burial as affected by mould-board design parameters, ploughing depth and speed: DEM simulations and experimental validation. Bio-systems Engineering. https://doi.org/10.1016/j.biosystemseng.2022.02.005

Bai CC (2010) Research and study on development trends of paddy tillage machinery in south China. Cor-pus ID: 111688637

Efremov AN, Nasonov SY (2016) Machines and technologies of entire lands levelling for paddy field. Tractors and Agricultural Machinery 83(3):37-42. https://doi.org/10.17816/0321-4443-66150

Fan YH, Zheng ML, Zhang DQ, Yang SC, Cheng MM (2011) Static and dynamic characteristic of cutting force when high-efficiency cutting Ti-6Al-4V. Advanced Materials Research 305: 122-128. https://doi.org/10.4028/www.scientific.net/AMR.305.122

Gupta JP, Singh S (2012) Design and development of rotary tiller blade. Agricultural Engineering International: CIGR Journal 14(2): 1-9. https://doi.org/10.1016/j.biosystemseng.2004.05.011

Hu L, Xu Y, He J, Du P, Luo X (2020) Design and test of tractor-attached laser-controlled rotary scraper land leveler for paddy fields. Journal of Irrigation and Drainage Engineering 146(4): 04020002. https://doi.org/10.1061/(ASCE)IR.1943-4774.0001448

Konno S, Shindo H, Katahira M, Natasuga M (2016) Fuel consumption of agricultural machines on paddy fields. Corpus ID: 209381702.

Matin MA, Fielke JM, Desbiolles J (2014) Furrow parameters in rotary strip-tillage: effect of blade geometry and rotary speed. Biosystems Engineering 118: 7-15. https://doi.org/10.1016/j.biosystemseng.2013.10.015

Matin MA, Desbiolles JMA, Fielke JM (2016) Strip-tillage using rotating straight blades: effect of cutting edge geometry on furrow parameters. Soil and Tillage Research 155: 271-279. https://doi.org/10.1016/j.still.2015.08.016

Mousavi SF, Yousefi-Moghadam S, Mostafazadeh-Fard B, Hemmat A, Yazdani MR (2009) Effect of puddling intensity on physical properties of a silty clay soil under laboratory and field conditions. Paddy and Water Environment 7(1): 45-54. https://doi.org/10.1007/s10333-008-0148-4

Shi Y, Sun XR, Wang X, Hu Z, Ding W (2019) Numerical simulation and field tests of minimum-tillage planter with straw smashing and strip laying based on EDEM software. Computers and Electronics in Agriculture 166(8): 105021. https://doi.org/10.1016/j.compag.2019.105021

Shrivastava A, Verma A, Ganguly SK (2015) Design of compound die for production of cutting blades for nonactive rotary paddy weeder. Materials and Manufacturing Processes 30(12): 1412-1416. https://doi.org/10.1080/10426914.2014.973601

Shrivastava A, Verma A (2017) Implementation of Taguchi methodology in optimization of developed jigs and fixtures for production of paddy weeder. Paddy and Water Environment 15: 1-9. https://doi.org/10.1007/s10333-016-0522-6

Singh Y, Singh VP, Singh G, Yadav DS, Sinha RKP, Johnson DE, Mortimer AM (2011) The implications of land preparation, crop establishment method and weed management on rice yield variation in the rice–wheat system in the Indo-Gangetic plains. Field Crops Research 121(1): 64-74. https://doi.org/10.1016/j.fcr.2010.11.012

Ucgul M, Saunders C (2020) Simulation of tillage forces and furrow profile during soil-mouldboard plough interaction using discrete element modelling. Biosystems Engineering 190: 58-70. https://doi.org/10.1016/j.biosystemseng.2019.11.022

Xin F, Xiao XM, Dong JW, Zhang GL, Zhang Y, Li B (2019) Large increases of paddy rice area, gross primary production, and grain production in Northeast China during 2000–2017. Science of The Total Environment 711: 135183. https://doi.org/10.1016/j.scitotenv.2019.135183

Zhao HB, Li HW, Ma SC, He J, Wang QJ, Lu CY, et al (2020) The effect of various edge-curve types of plain-straight blades for strip tillage seeding on torque and soil disturbance using DEM. Soil & Tillage Research 202: 104674. https://doi.org/10.1016/j.still.2020.104674

Zhou H, Hu L, Luo X, Tang L, Du P, Mao T, Zhao R, He J (2020) Design and test of laser-controlled paddy field levelling-beater. International Journal of Agricultural and Biological Engineering 13(1): 57-65. https://doi.org/10.25165/j.ijabe.20201301.4989

Zhu HZ, Zhong H, Wu JL (2016) Incorporating rice residues into paddy soils affects methylmercury accumulation in rice. Chemosphere 152: 259-264. https://doi.org/10.1016/j.chemosphere.2016.02.095